SSRG International Journal of Recent Engineering Science
ISSN: 2349–7157 / https://doi.org/10.14445/23497157/IJRES-V11I3P108

Volume 11 Issue 3, 77-88, May-Jun 2024

Original Article

NaOH Activated Carbon Prepared from Millet Husk and Millet Straw for Heavy Metals Adsorption: Isotherms and Kinetics Studies

Burah Tijjani[1*], Ali Lawan Yaumi[2], Hamza Umar[2], Mohammed Modu Aji[2], Bitrus Kwaji Highina[2]

[1]*Department of Chemical Engineering, Federal University of Technology Owerri, Imo State, Nigeria.*
[2]*Department of Chemical Engineering, University of Maiduguri, Borno State, Nigeria.*

[1]*Corresponding Author : brahtijjani@gmail.com*

Received: 11 April 2024 Revised: 16 May 2024 Accepted: 27 May 2024 Published: 15 June 2024

Abstract *- Raw Millet Husk (RMH) and Raw Millet Straw (RMS) were used as precursors and were carbonized; they were further activated with Sodium Hydroxide (NaOH) to obtain Millet Husk and Straw (MHS) activated carbon. The industrial effluent sample was analyzed before and after Adsorption by Atomic Absorption Spectrometry (AAS). The experimental data were fitted to Langmuir and Freundlich isotherm models. Adsorption data of lead, arsenic and mercury were well fitted with the Freundlich model as indicated by higher values of Regression coefficient R^2. The agreement of the Freundlich model to the experimental data may designate multilayer adsorption had taken place on the MHS surface that could contain a finite number of identical sites. The experimental kinetics data was analyzed using pseudo-first-order, Pseudo-second-order, Elovich and intraparticle diffusion. The pseudo-second-order kinetic model provided a better Correlation for the experimental data, indicating a chemisorption process. This proposes that the forming of the interface between the adsorbate and the adsorbent on the external surface of the adsorbent (film diffusion) is the rate-determining step.*

Keywords *- Millet husk, Millet straw, Heavy metals, Adsorption, Kinetics.*

1. Introduction

Because of the accelerated rate of urbanization and growth, as well as the discharge of industrial and municipal effluents that threaten the survival of aquatic life, rivers are under excessive stress (Khan et al., 2021). However, untreated wastewater released by industries is the main cause of water contamination. Among the toxins present in industrial wastewater that find their way into the environment are dyes, aromatics, pesticides, heavy metals, oil, and other hazardous substances that pose a major risk to both human health and the ecosystem (Nallakukkala et al., 2022).

Both anthropogenic (sewerage systems, home and industrial wastewater) and natural (geological weathering, precipitation) sources of metal contamination are likely present in freshwater habitats. Heavy Metals (HMs) have a persistent non-biodegradable character that can cause bio-accumulation and biomagnification when they enter the food chain. At locations far from the source of contamination, the interaction between Heavy Metals (HMs) and natural water can modify the concentration and extent of the HMs' harmful effects. Given that rivers are the main inland water resources used for human sustenance, effective monitoring and management of the water quality in these bodies of water is, therefore, essential (Khan et al., 2021). Heavy metals are very soluble in water, which allows living things to absorb them. Once heavy metals enter the food chain, they have the potential to accumulate significantly in the human body. Metal overconsumption beyond the permitted concentration limit can lead to detrimental health effects. Therefore, wastewater contaminated with heavy metals needs to be cleaned before being released into the environment (Nallakukkala et al., 2022).

To remove heavy metals from inorganic wastewater, conventional treatment techniques such as adsorption, membrane, chemical precipitation, and electrochemical approaches are employed. Although these methods are reliable, they have significant drawbacks, such as low selectivity, restricted metal removal, high energy requirements, and significant sludge production. A variety of techniques have recently been studied in an effort to improve treated water quality while simultaneously reducing the amount of wastewater produced cost-effectively and efficiently (Nallakukkala et al., 2022). Owing to its low cost of reusability, robust application, high removal rate, and ease of operation, adsorption is the most promising technique for removing heavy metal ions from wastewater that has

received extensive research. This choice is contingent upon the selection of inexpensive materials, high absorption rates, and effective regeneration mechanisms. Chemical, adsorption, and membrane techniques are typically the most useful ones discussed in the literature (Qasem & Mohammed, 2021).

There have been trials conducted on a variety of agricultural by-products, including rice bran, rice husk, wheat bran, sawdust from different plants, tree bark, groundnut shells, coconut shells, back gramme husk, hazel nut shells, walnut shells, cotton seed hulls, millet husk, waste tree leaves, maize corn cob, sugarcane bagasse, banana, orange peels, soya bean hulls, grapes stalks, water hyacinth, sugar beet pulp, sunflower stalks, coffee bean, cotton stalk, etc (Batagarawa et al., 2017). In Nigeria, an estimated 2.76 million tonnes of millet plant residue are produced annually (Ajikashile et al., 2023). Every year, a significant amount of crop residues—such as sorghum husk, millet husk, cowpea husk, maize bran, wheat bran, groundnut halves, maize cobs and maize straw—produced on government and private farms in Nigeria are thrown away. Some are burned, while some are allowed to rot in the field, which may increase soil fertility (Millam, 2018). Among the millions of tonnes of agricultural waste looking for a way out are millet husks. Millet husk's renewable, biodegradable, lightweight, and economical qualities make it an appealing material (Abba et al., 2017). In local agricultural fields, millet husk is abundant and regarded as waste following grain separation (Das et al., 2018). Similar to wheat and rice straw, there is no other documented commercial utility for millet straw (Karimi & Tavakkoli, 2019). Consequently, this study presents the preparation of NaOH-activated carbon from Millet Husk and Millet Straw (MHS) and its application for heavy metals adsorption from industrial effluent. In addition, the Isotherm and kinetics of the adsorption process will be evaluated using Langmuir, Freundlich, Pseudo-first-order, Pseudo-second-order, Elovich and Intraparticle diffusion models to ascertain the nature and mechanism of the adsorption process.

2. Materials and Method

2.1. Sample Collection

The sample effluent was collected in a 5-litre polyethene can from the Coca-Cola Bottling Company, Maiduguri, Borno State, Nigeria. The polyethene can was washed thoroughly with hot boiled water to get rid of foreign contaminants before the collection of the sample.

2.2. Sample Treatment

The millet husk was handpicked to remove dirty particles and washed with tap water severally to get rid of adhering particles. The millet straws were cut into pieces and were similarly washed several times with water to remove moisture-soluble impurities. Both samples were rewashed thoroughly with distilled water, drained, and sun-dried for 12 hours. The dried samples were stored in air-tight containers for further analysis.

2.3. Preparation of NaOH – Activated Carbon

Activated Carbons were prepared from the dried Millet Husk (MH) and Millet Straw (MS) using the chemical activation method. The dried samples were carbonized at 500°C for 2 hours in muffle furnaces to obtain a carbonized char. The obtained char was activated using NaOH at different ratios. The different mass ratios of powdered MH and MS to NaOH activation agent (1:2, 1:3 and 1:4) were taken and impregnated. It is then mixed thoroughly and allowed for 48 h at room temperature. A similar procedure was followed to impregnate the Millet Straw (MS). After impregnation, samples were then filtered and oven-dried at 105°C for 90 minutes so as to remove moisture completely. The activated carbons produced were washed with 0.5 M HCl acid solution, filtered and washed several times with distilled water to obtain a fairly constant pH. The samples were oven-dried at 250°C and labelled MH_1, MH_2, and MH_3 for millet husk and MS_1, MS_2 and MS_3 for millet straw with subscripts of their corresponding impregnated molarities. Such washing steps were required to eliminate metallic sodium, possible excesses of hydroxide, and soluble impurities present in the char (Byamba-ochir et al., 2016). A composite adsorbent (1M MH, 2M MH, 1M MS and 3M MS) was produced based on their performance from the first experiments. The heavy metals (As, Pb and Hg) present in samples were determined by using the Atomic Absorption Spectrophotometric (AAS) method. The adsorption equilibrium was investigated for different metal concentrations between 20 and 140mg/L. In addition, kinetics experiments were conducted with 20 – 140 mg/L metal and 0.1 g of adsorbent at 25^0C, temperature with stirring at 250 rpm for 20 – 120 min.

2.4. Adsorption Isotherm Models

2.4.1. Langmuir Isotherm Model

The Langmuir isotherm is used to describe monolayer sorption onto the surface of an adsorbent with a finite number of identical adsorption sites and no interaction between sites. The model is expressed by (Tatah et al., 2017):

$$\frac{C_e}{q_e} = \frac{1}{q_m K_L} + \frac{C_e}{q_m}, \qquad (1)$$

q_m (mg/g) = monolayer adsorption capacity of the adsorbent, K_L (L/mg)= adsorption constant, which reflects the affinity between the adsorbent and adsorbate. q_m and K_L were determined from the slope and intercept of the plots of Ce/qe versus Ce.

2.4.2. Freundlich Isotherm Model

The Freundlich adsorption isotherm model describes the reversible and non-ideal adsorption process. The Freundlich model can be applied to multilayer adsorption, unlike the Langmuir isotherm model, which is limited to monolayer creation.

The linearized form is:

$$logq_e = logK_F + \frac{1}{n}logC_e \quad (2)$$

Where $q_e$is the equilibrium amount adsorbed per unit mass of adsorbent (mg/g), C_e is the equilibrium concentration of the adsorbate in solution (mg/L); K_F is the Freundlich isotherm constant (L/mg), and n is adsorption intensity (Alaqarbeh, 2021).

2.5. Kinetics Study

Kinetics is a significant factor in the determination of the adsorption mechanism. In order to investigate the adsorption behavior deeply, pseudo-first-order, pseudo second order, Elovich and intraparticle diffusion kinetics models were used to analyze the experimentally obtained data and can be summarized as follows. The linear equations of pseudo-first-order, pseudo-second-order, Elovich and intraparticle kinetics models are as follows:

The pseudo-first-order with the boundary conditions as follows: t = 0, q_t = 0, and at t = t, $q_t = q_t$, gives:

$$ln(q_e - q_t) = lnq_e - k_1 t \quad 2.3$$

Where q_e and q_t are the values of the amount adsorbed per unit mass on the adsorbent at equilibrium and at various times *t*, respectively; k_1 is the Pseudo-first-order adsorption rate constant (min^{-1}). The values of k_1 and calculated q_e can be determined from the slope and intercept, respectively, of the linear plot of $ln(q_e - q_t)$ versus *t.*

Pseudo-second-order with the boundary conditions $t = 0$, q_t= 0, and at $t = t$, $q = q$, results in:

$$\frac{t}{q_t} = \frac{t}{q_e} + \frac{1}{k_2 q_e^2} \quad 2.4$$

Where k_2 is the pseudo-second-order adsorption rate constant (g/mg. min), q_e and q_t are the amount adsorbed (mg/g) on the adsorbent at equilibrium and at time t.

Elovich kinetics model with *t* value at $t_o \rightarrow t$ and q_t value point in saturate adsorbent capacity (mg/g):

$$q_t = \frac{1}{\beta}ln(\alpha\beta) + \frac{1}{\beta}\ln(t + t_o) \quad 2.5$$

Where α is the initial adsorption rate (mg/min), and β is the surface coverage and energy to interact with the chemisorption process. To evaluate kinetic surface interference with adsorbent plot linearly against q_t vs. $\ln(t + t_o)$ and the Elovich coefficients, α and β, calculate slope and intercept.

Intraparticle diffusion:

$$q_t = K_{id}t^{1/2} + C \quad 2.6$$

Where K_{id} is the intraparticle rate constant (mg L^{-1} $min^{-1/2}$), and C is the thickness of the boundary layer. The model calculates from a linear plot against the of q_t vs. $t^{1/2}$.

3. Results and Discussion

3.1. Isotherms Study

Adsorption isotherms allow evaluating the applicability of the adsorption process as a unit operation and estimating the maximum adsorption capacities of adsorbent materials. Moreover, the fit of the isotherm models to the experimental data provides information about the nature of the adsorption process. The adsorption parameters were determined by using linearized Langmuir and Freundlich isotherm models. Table 3.1 presents the isotherm parameters, while Figure 4.9 (a-c) shows the experimental data fitted to the Langmuir and Freundlich isotherm models for the removal of Pb, As, and Hg using MHS.

According to Table 3.1 and Figure 3.1(a-c), the Freundlich model had a better fit to the experimental data than the Langmuir model, considering the correlation coefficients, R^2 values of Pb, As, and Hg, which is 0.9999, 0.9985 and 0.9995 respectively. The agreement of the Freundlich model to the experimental data may designate multilayer adsorption had taken place on the MHS surface that could contain a finite number of identical sites. In addition, the values of n (0.926 and 0.914) for Pb and As on MHS were less than 1 (n<1), suggesting that the adsorption process is more likely to be chemical, indicating strong interactions between the adsorbates (Pb and As) and the adsorbent. On the other hand, the value of n (1.051) for Hg on MHS was greater than 1 (n>1), which indicates that the system is more heterogeneous, which leads to non-linearity of the isotherm. The larger value of n implies stronger adsorption intensity, meaning that more adsorption occurs per unit mass of the adsorbent at relatively low concentrations or pressures (Tatah et al., 2017). The high value of n indicates a relatively uniform surface where low values mean high adsorption at low concentrations of solution. In addition, low values of n indicate the existence of a high proportion of high-energy active sites (Adres et al., 2022). A higher value of 1/n indicates an unfavorable adsorption process. Moreover, the values of K_F were found to be 1.407, 1.593 and 1.006 L/g, implying that there was high uptake of the metal ions onto the MHS surface. The higher the value of K_F, the greater the adsorption intensity (Vaishnav et al., 2012).

Although, the Langmuir separation factors (R_L= 0.022, 0.017, 0.050) for the adsorption of Pb, As and Hg onto MHS, respectively, indicate that the adsorption process is favorable (Shi et al., 2019). It was observed in this study that the Langmuir adsorption model provided a poor fit to the equilibrium data as compared to the Freundlich model. This

was indicated by the low correlation coefficient (R^2) values 0.3434, 0.3290, and 0.3851 on MHS for Pb, As and Hg, respectively, which implied that the adsorption process of Pb, As, and Hg onto MHS is not monolayer rather it is multilayer. The Langmuir separation factor (R_L) is used to evaluate the feasibility of the adsorption process, indicating when the adsorption is unfavorable ($R_L > 1$), linear ($R_L = 1$), favorable ($0 < R_L > 1$) or irreversible ($R_L = 0$) (Harrache et al., 2018). A similar result was reported by Junejo et al. (2019), where Reactive Blue (RB-19) Dye was adsorbed using Calix (4) arene-based adsorbent.

Table 3.1. Isotherm parameters for the adsorption of heavy metals onto MHS

Models/Parameters	Lead	Arsenic	Mercury
Langmuir			
q_{max}(mg/g)	201.423	140.213	259.038
K_L (L/mg)	2.264	2.969	0.945
R_L	0.022	0.017	0.050
R^2	0.3434	0.3289	0.3851
Freundlich			
K_f (L/g)	1.407	1.593	1.006
1/n	1.080	1.095	0.951
N	0.926	0.914	1.051
R^2	0.9999	0.9985	0.9995

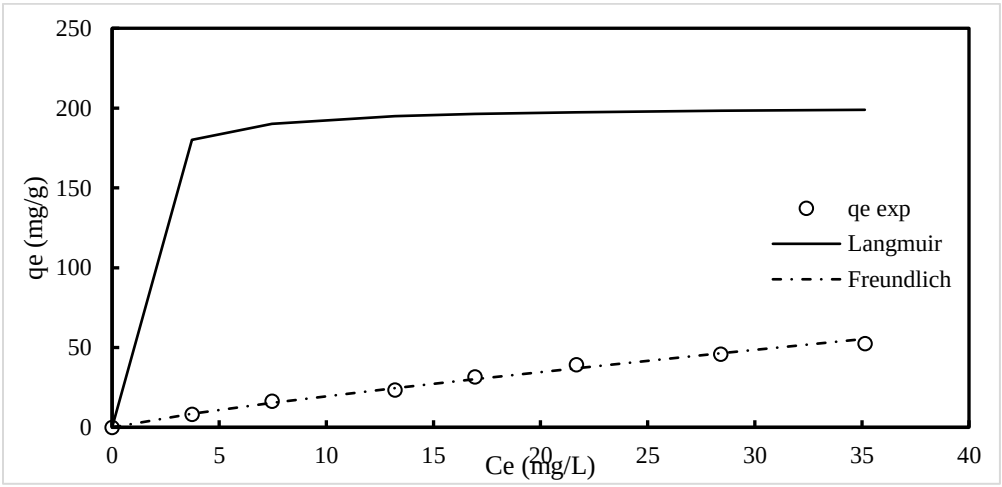

Fig. 3.1a Langmuir and freundlich isotherms for Pb adsorption by MHS

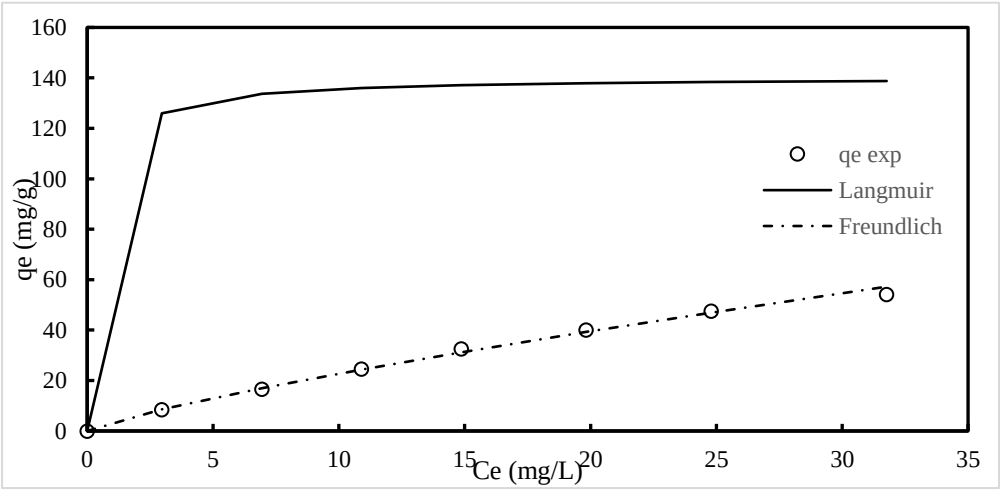

Fig. 3.1b Langmuir and freundlich isotherms for as adsorption by MHS

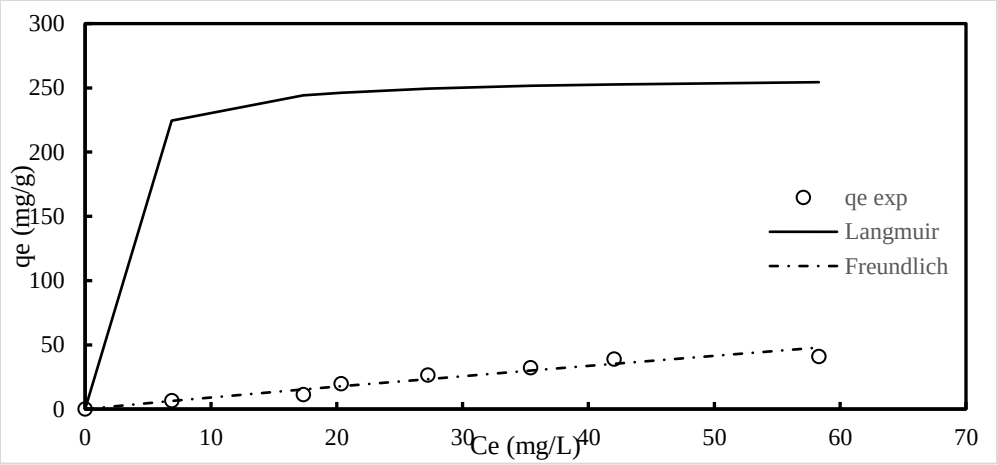

Fig. 3.1c Langmuir and Freundlich isotherms for Hg adsorption by MHS

3.2. Kinetics Study

Four kinetic models, Pseudo-First-Order, Pseudo-Second-Order, Elovich, and Intraparticle diffusion model, with initial concentrations of 20–140 mg/L, at different time intervals and temperature of 25°C were applied to study the reaction pathways and potential rate-determining steps of the adsorption of Pb, As, and Hg onto MHS. Table 3.2(a-d) summarized the kinetics parameters, whereas Figure 3.2(a-l) presented the plots of the kinetics study.

The pseudo-second-order model exhibits better fitting of the kinetic data due to the excellent linearity with high correlation coefficients, $R^{2,}$ for the adsorption of Pb, As, and Hg on MHS, unlike the pseudo-first-order model. Further, the agreement between the calculated *qe* and the experimental *qe* values is very good because the differences are less, signifying that the adsorption of Pb, As, and Hg by MHS is better fitted to the pseudo-second-order kinetic. Thus, the adsorption process is controlled by chemisorption. This proposes that the forming of the interface between the adsorbate and the adsorbent on the external surface of the adsorbent (film diffusion) is the rate-determining step. Additionally, the fitness of pseudo-second-order indicates that chemical interaction was involved in the adsorption process of Pb, As and Hg onto the activated carbons (Bello et al., 2020).

However, the pseudo-first-order model did not provide a good fit for the experimental data. Table 3.1(a-c) showed low correlation coefficient, R^2 values and the wide differences between the calculated and experimental equilibrium adsorption capacities *qe* of the pseudo-first-order model as compared to the pseudo-second-order model, implying the insufficiency of the pseudo-first-order model for describing the adsorption kinetics of Pb, As, and Hg onto MHS. The Elovich model with moderate R^2, α, and β values, as shown in Table 3.1(a-c), suggests that the mechanism is not entirely a chemosorption. Figure 3.1(g-i) shows that the Elovich model is linear at lower concentrations and nonlinear at higher concentrations. When the Elovich model is linear at lower concentrations of the adsorbate, it means that the relationship between the rate of the adsorption and the concentration of the adsorbate follows a straight line; this suggests that at low concentrations, the adsorption process is relatively straightforward and predictable. The rate of adsorption increases linearly with increasing concentration.

Conversely, when the Elovich model becomes nonlinear at higher concentrations, it indicates that the relationship between the rate of adsorption and the concentration of the adsorbate deviates from a simple linear trend. At higher concentrations, additional factors come into play. These might include surface saturation, interactions between adsorbed molecules or changes in the adsorption mechanism. The nonlinearity suggests that the adsorption process becomes more complex as the concentration of the adsorbate increases (Ayawei et al., 2017). Moreover, the intraparticle diffusion model did not provide a good fit for the experimental data. The intraparticle diffusion rate constant, K_{id}, the intercept, C and the correlation coefficients, R^2 are given in Table 3.1(d). Figure 3.1(j-l) gives a linear relationship at lower concentrations of adsorbate and a nonlinear at higher concentrations, which indicates a change in the adsorption process based on the concentration levels. At low concentrations, the model shows a linear relationship between the adsorbate concentration and the rate of intraparticle diffusion, suggesting a consistent diffusion process. Conversely, at higher concentrations, this relationship becomes nonlinear, implying that intraparticle diffusion is no longer solely dependent on the concentration but may be influenced by other factors, such as saturation of adsorption sites or changes in the diffusion mechanism (Karapanagioti et al., 2001). According to the model, a plot of qt versus $t^{1/2}$ yields a straight line whose slope corresponds to the intraparticle diffusion rate constant (K_{id}), and the intercept (C) gives insights into the thickness of the boundary layer around the adsorbent particles. If the plot exhibits a

linear trend, intraparticle diffusion plays a dominant role in controlling the adsorption process. On the contrary, if the plot shows a departure from linearity, other mechanisms, such as film diffusion or chemical adsorption, contribute significantly to the overall adsorption process (Guo and Wang, 2022).

Table 3.2a. Kinetic parameters for adsorption of Pb onto MHS

		Pseudo-First-Order			Pseudo-Second-Order			Elovich		
Co (mg/L)	qe exp (mg/g)	K_1 (1/hr)	qe cal (mg/g)	R^2	K_2 (g/mg.min)	qe cal (mg/g)	R^2	β (mg/g)	α (mg/min)	R^2
20	8.135	0.007	0.770	0.7433	0.215	7.782	0.9998	0.829	1.639	0.8800
40	16.267	0.017	1.152	0.9671	-0.005	18.797	0.9649	-2.298	3.945	0.6635
60	23.400	0.006	0.821	0.9033	0.099	22.883	0.9999	2.467	4.827	0.8780
80	31.533	-0.004	1.041	0.7913	0.175	30.864	1.0000	3.399	6.536	0.8744
100	39.166	0.011	0.962	0.8266	0.114	38.911	1.0000	4.287	8.234	0.8741
120	45.799	0.024	1.112	0.8773	0.100	45.662	1.0000	5.027	9.686	0.8748
140	52.432	0.013	1.053	0.9019	0.091	52.356	1.0000	5.733	11.058	0.8750

Table 3.2b. Kinetic parameters for adsorption of As onto MHS

		Pseudo-First-Order			Pseudo-Second-Order			Elovich		
Co (mg/L)	qe exp (mg/g)	K_1 (1/hr)	qe cal (mg/g)	R2	K_2 (g/mg.min)	qe cal (mg/g)	R2	β (mg/g)	α (mg/min)	R2
20	8.517	0.009	0.887	0.9193	0.158	8.183	0.9999	0.808	1.729	0.8958
40	16.529	0.025	1.986	0.8218	-0.005	18.939	0.9668	-2.351	3.932	0.6704
60	24.550	0.014	0.539	0.2540	0.251	24.390	0.9999	2.646	5.175	0.8779
80	32.567	0.003	1.030	0.3970	0.397	31.746	1.0000	3.518	6.745	0.8736
100	40.084	0.021	0.487	0.5780	0.625	40.000	1.0000	4.483	8.484	0.8708
120	47.601	0.012	1.010	0.7334	0.111	47.393	1.0000	5.180	10.031	0.8758
140	54.118	0.005	1.078	0.8055	0.130	53.476	1.0000	5.934	11.343	0.8730

Table 3.2c. Kinetic parameters for adsorption of Hg onto MHS

		Pseudo-First-Order			Pseudo-Second-Order			Elovich		
Co (mg/L)	qe exp (mg/g)	K_1 (1/hr)	qe cal (mg/g)	R^2	K_2 (g/mg.min)	qe cal (mg/g)	R^2	β (mg/g)	α (mg/min)	R^2
20	5.562	0.034	5.039	0.3507	0.664	5.540	0.9997	0.620	1.169	0.8691
40	11.340	0.029	1.650	0.5286	0.007	12.837	0.9653	1.569	2.686	0.6642
60	19.829	0.013	0.605	0.3108	0.141	19.685	0.9998	2.141	4.158	0.8760
80	26.395	0.031	1.006	0.9012	0.129	26.385	1.0000	2.871	5.584	0.8768
100	32.310	0.031	1.583	0.5202	0.099	32.154	0.9997	3.502	6.794	0.8759
120	38.987	0.015	0.991	0.9192	0.099	38.911	1.0000	4.259	8.216	0.8750
140	40.848	0.048	1.333	0.8549	0.182	40.816	1.0000	4.549	8.654	0.8720

Table 3.2d. Intraparticle diffusion constants for Pb, As and Hg onto MHS

	Pb			As			Hg		
Co (mg/L)	K_{id}	R^2	C	K_{id}	R^2	C	K_{id}	R^2	C
20	0.636	0.6791	2.176	0.675	0.6996	2.201	1.338	0.6641	1.596
40	1.963	0.7381	-1.565	1.965	0.7526	-1.676	1.610	0.7398	1.075
60	1.870	0.6750	6.458	2.003	0.6733	6.941	2.161	0.6727	5.584
80	2.526	0.6688	8.847	2.605	0.6674	9.152	3.177	0.6727	7.503
100	3.182	0.6687	11.149	3.272	0.6635	11.599	2.629	0.6717	9.142
120	3.744	0.6696	13.092	3.879	0.6708	13.525	3.177	0.6701	11.094
140	4.275	0.6698	14.939	4.380	0.6670	15.407	3.341	0.6655	11.788

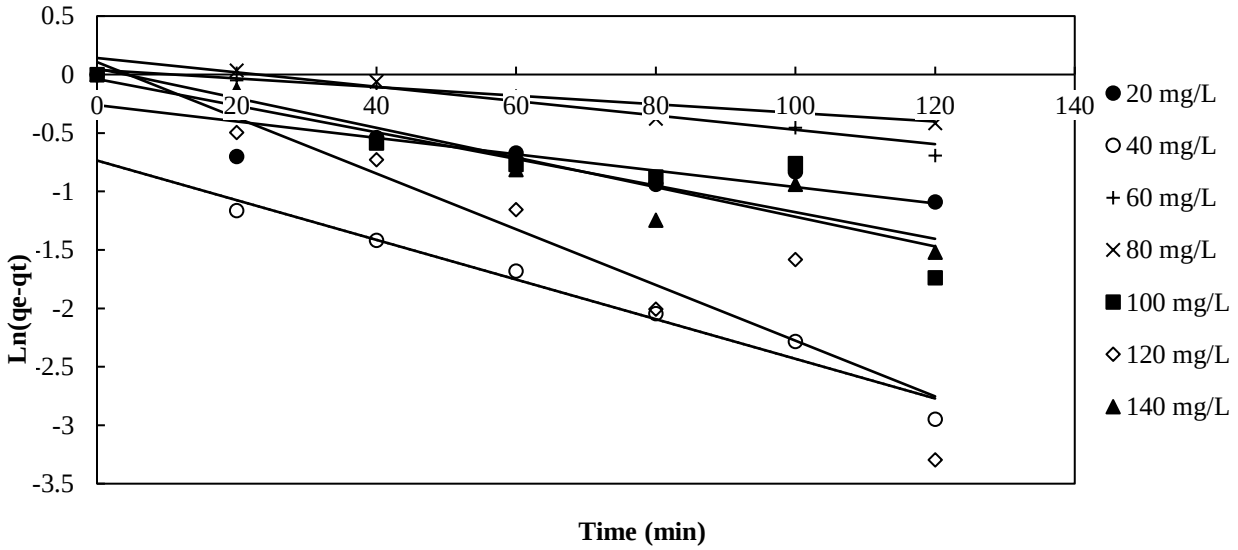

Fig. 3.2a Pseudo-first-order plot of Pb onto MHS.

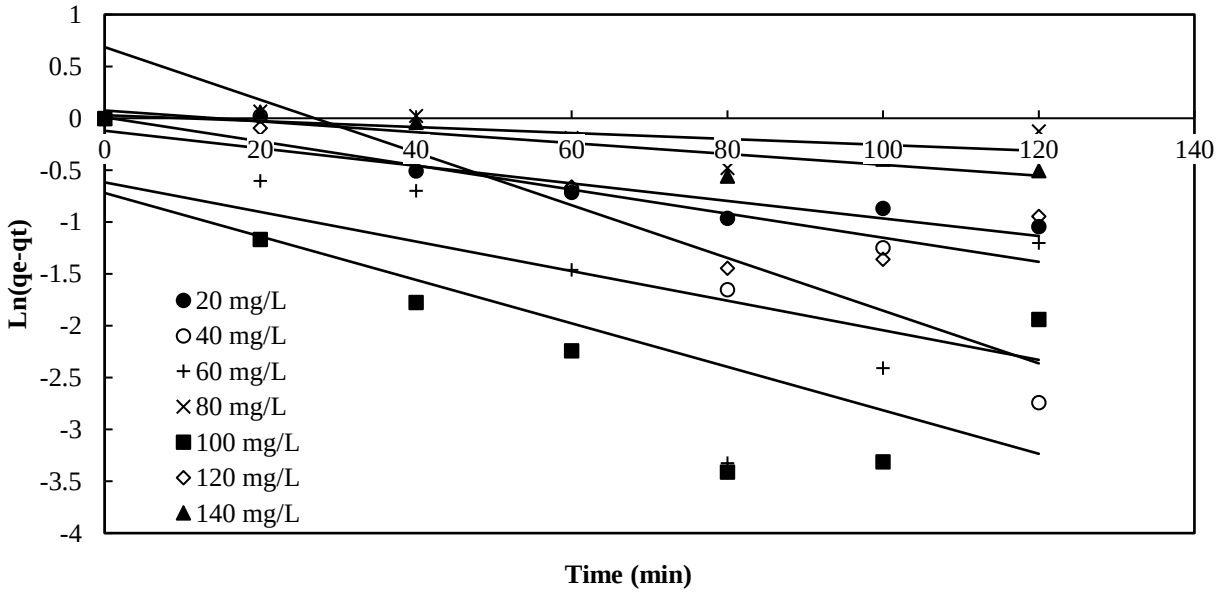

Fig. 3.2b Pseudo-first-order plot of As onto MHS.

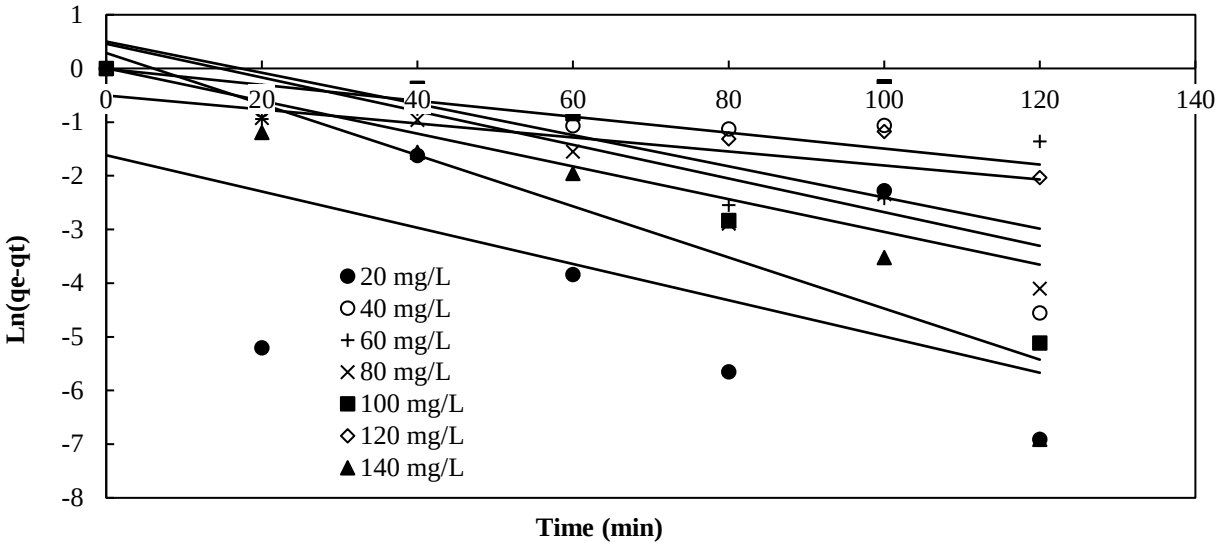

Fig. 3.2c Pseudo-first-order plot of Hg onto MHS

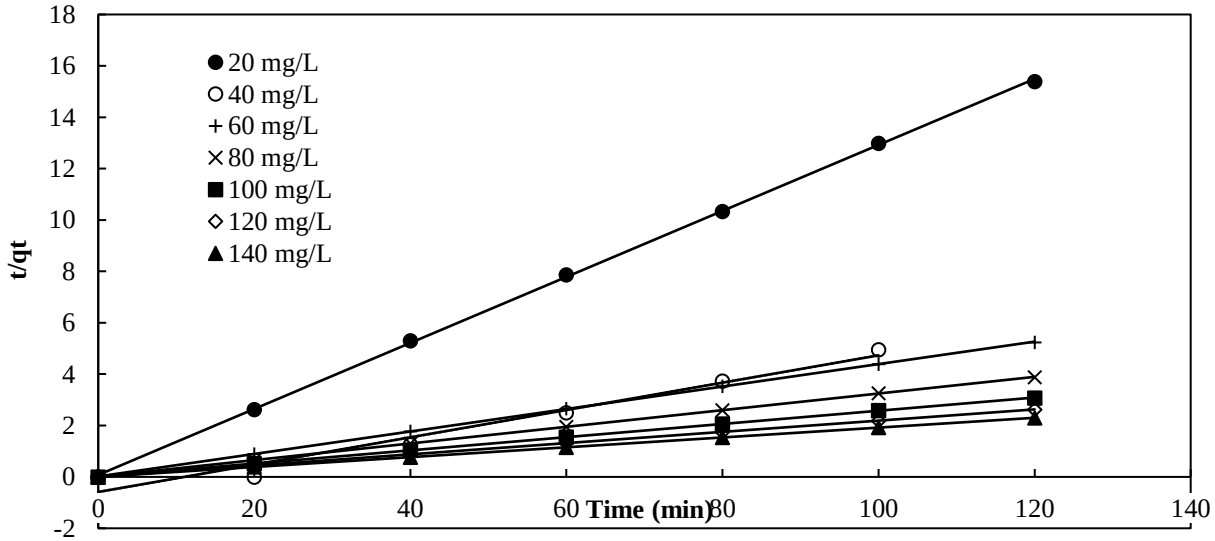

Fig. 3.2d Pseudo-second-order plot of Pb onto MHS.

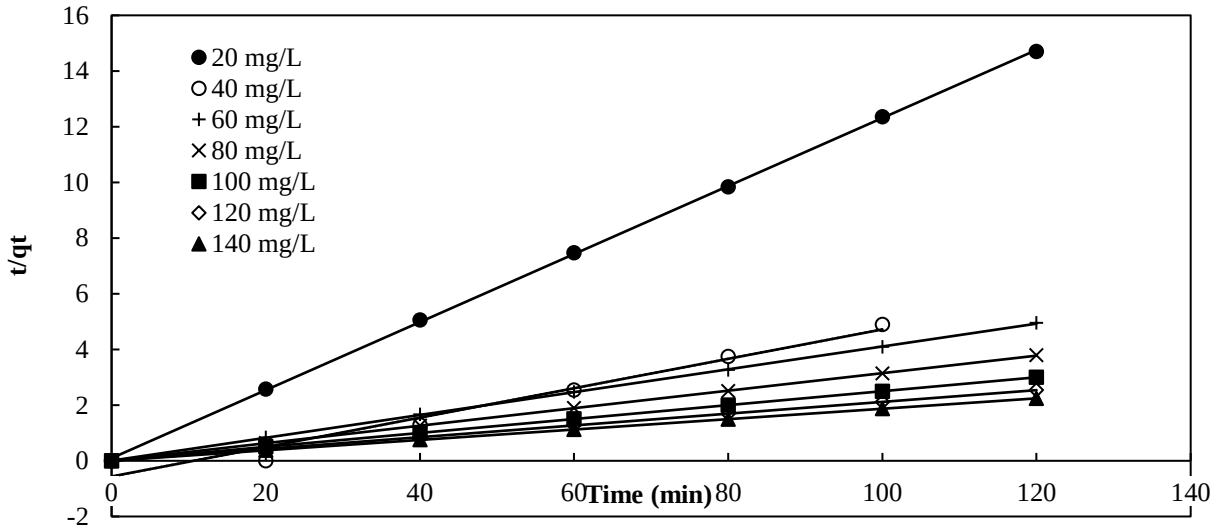

Fig. 3.2e Pseudo-second-order plot of As onto MHS.

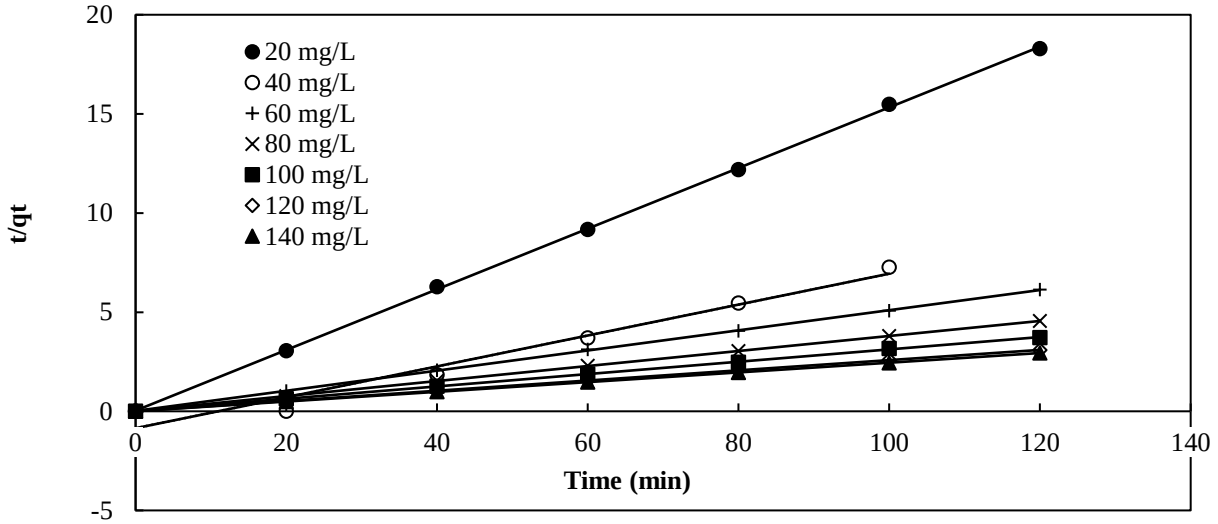

Fig. 3.2f Pseudo-second-order plot of Hg onto MHS

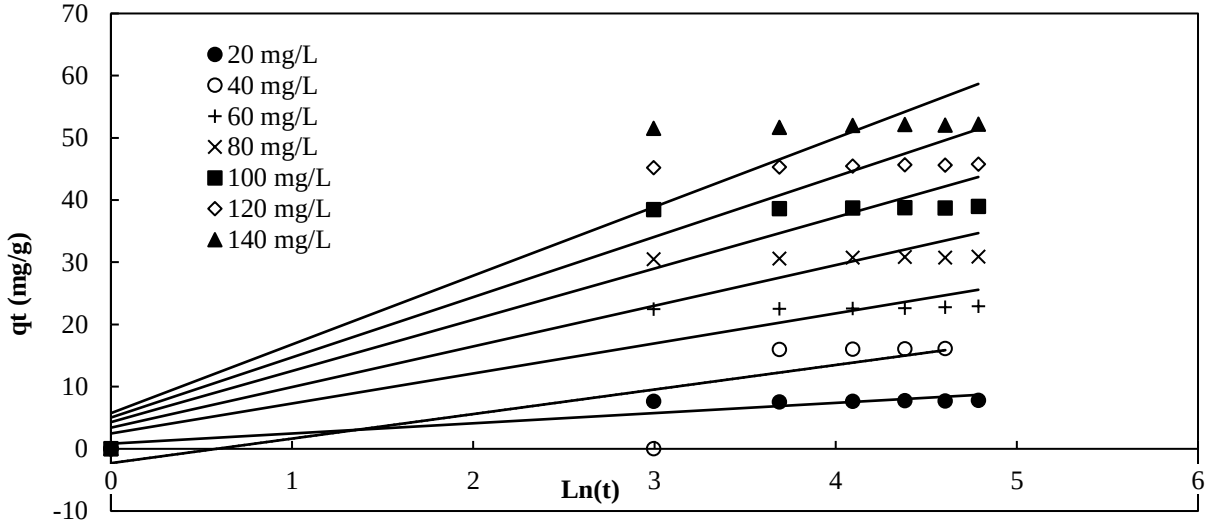

Fig. 3.2g Elovich plot of Pb onto MHS.

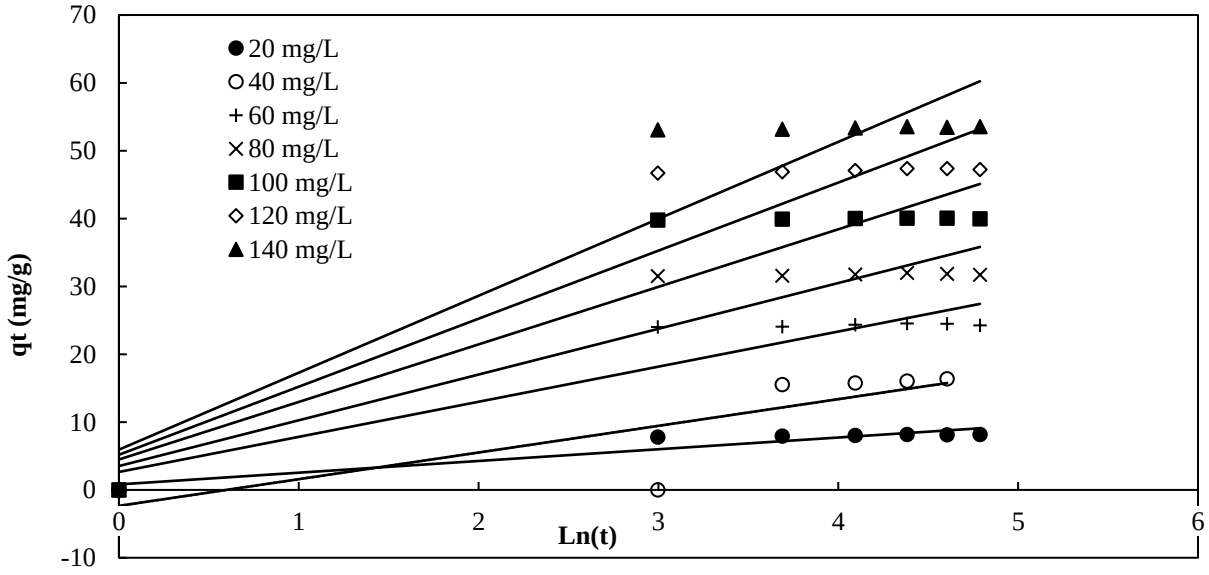

Fig. 3.2h Elovich plot of As onto MHS

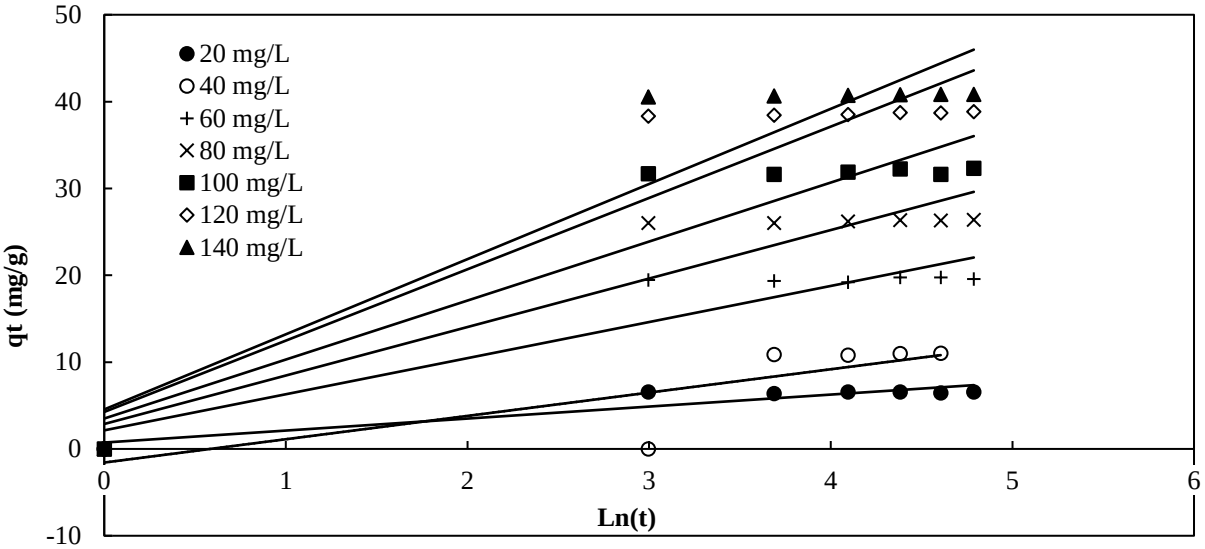

Fig. 3.2i Elovich plot of Hg onto MHS.

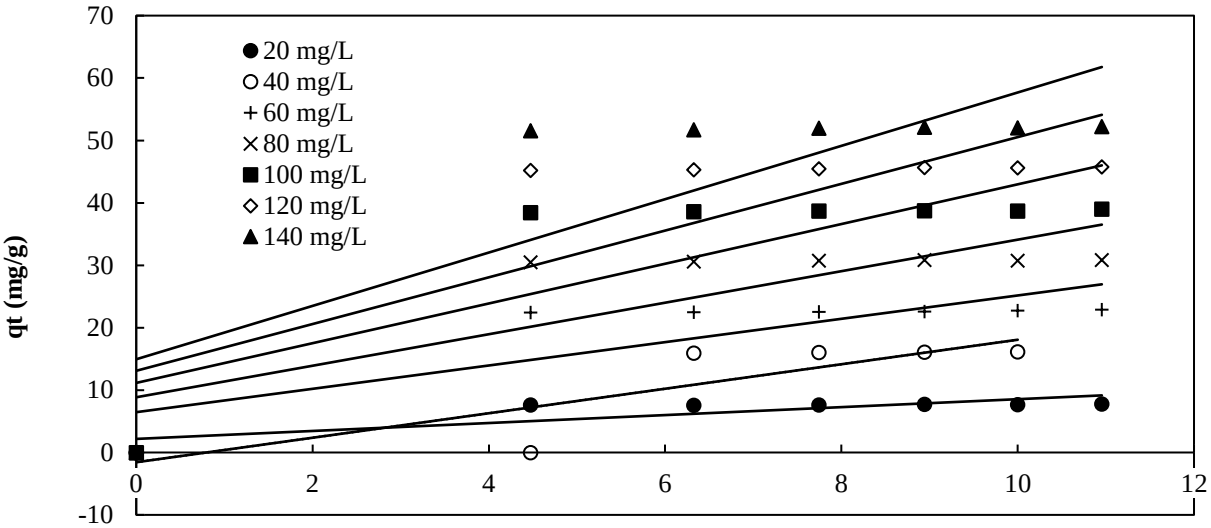

Fig. 3.2j Intraparticle diffusion plot of Pb onto MHS.

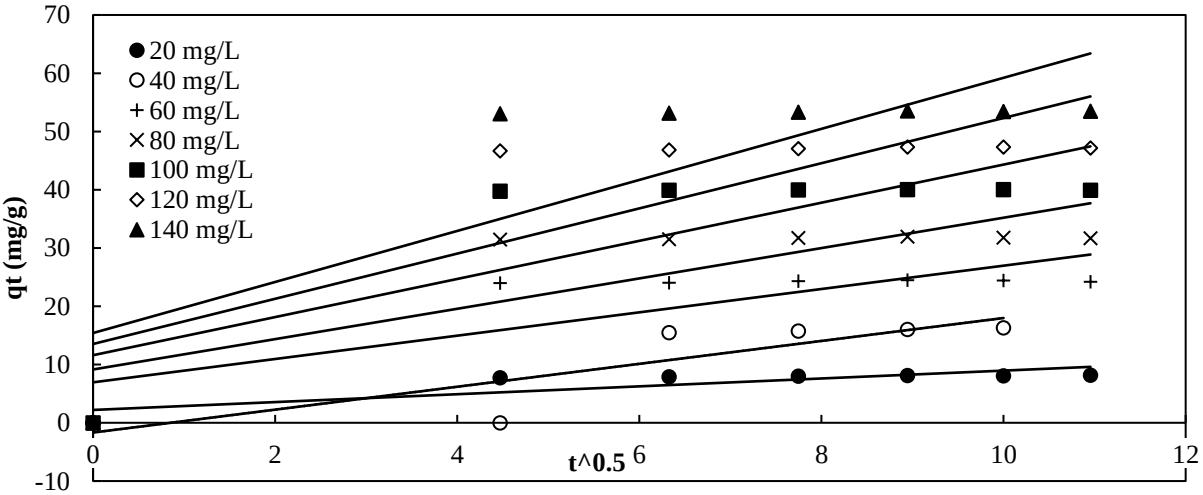

Fig. 3.2k Intraparticle diffusion plot of As onto MHS

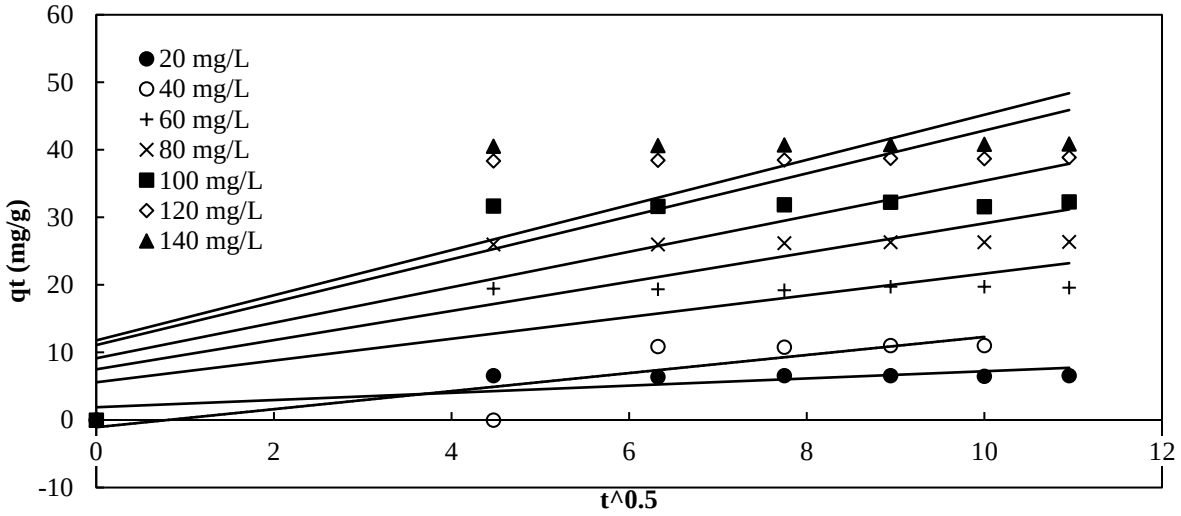

Fig. 3.2l Intraparticle diffusion plot of As onto MHS.

4. Conclusion

The adsorption isotherms and kinetics of NaOH based activated carbon were examined in this study. The industrial effluent sample was analyzed before and after adsorption by Atomic Adsorption Spectrometry (AAS). The experimental data were fitted to Isotherms and kinetics models (Langmuir, Freundlich, Pseudo-first-order, Pseudo-second-order, Elovich and Intraparticle diffusion). The result revealed that the adsorption data of lead, arsenic and mercury were well fitted with the Freundlich model as indicated by higher values of Regression coefficient $R^{2,}$ suggesting multilayer adsorption had taken place on the MHS surface of the adsorbent. In contrast, the Pseudo- -Second-Order Kinetic model had a better correlation with experimental data for all the metal ions, thus signifying a chemisorption process on the surface of MHS.

Funding Statement

The authors of this research used their funds to conduct the work and publish the article.

Acknowledgements

All the Authors contributed jointly to the success of this work.

References

[1] Abba A. Hammajam et al., "Characterization of Millet (Pennisetum glaucum) Husk Fiber (MHF) and Its Use as Filler for High Density Polyethylene (HDPE) Composites," *BioResources,* vol. 12, no. 4, pp. 9287-9301, 2017. [Google Scholar] [Publisher Link]

[2] Narain Das Bheel et al., "Millet Husk Ash as Environmental Friendly Material in Cement Concrete," *5th International Conference on Energy, Environment and Sustainable Development (EESD)*, pp. 153–158, 2018. [Google Scholar]

[3] H. Büyükgüngor, and Y. Orhan, "The Removal of Heavy Metals by Using Agricultural Wastes," *Water Science and Technology*, vol. 28, no. 2, pp. 247-255, 2018. [CrossRef] [Google Scholar] [Publisher Link]

[4] J.J. Millam et al., "Development of Feeding Regimes with Some Crop Residues : Maize Offal, Cowpea Husk, Poultry Litter and Groundnut Haulms in a Semi-arid Environment of Nigeria," *Nigerian Journal of Animal Science,* vol. 20, no. 3, 2018. [Google Scholar] [Publisher Link]

[5] Joshua Oluyinka Ajikashile et al., "The Influence of Torrefaction Temperature and Reaction Time on the Properties of Torrefied Sun-dried Millet and Sorghum Straws from the Arid and Semi-arid Zones of Western Africa," *Biofuels, Bioproducts and Biorefining,* vol. 17, no. 3, pp. 751–767, 2023. [CrossRef] [Google Scholar] [Publisher Link]

[6] Jie Shi et al., "Enhanced Adsorption of As (III) on Chemically Modified Activated Carbon Fibers," *Applied Water Science*, vol. 9, 2019. [CrossRef] [Google Scholar] [Publisher Link]

[7] Marwa Alaqarbeh, "Adsorption Phenomena : Definition, Mechanisms, and Adsorption Types : Short Review," *Green and Applied Chemistry*, vol. 13, 2021. [CrossRef] [Google Scholar] [Publisher Link]

[8] Mojeed O. Bello et al., "Isotherm and Kinetic Studies of Adsorption of Methylene Blue Using Activated Carbon from Ackee Apple Pods," *Chemical Data Collections*, vol. 31, 2021. [CrossRef] [Google Scholar] [Publisher Link]

[9] Naef A.A. Qasem, Ramy H. Mohammed, and Dahiru U. Lawal, "Removal of Heavy Metal Ions from Wastewater : A Comprehensive and Critical Review," *Nature Partner Journals Clean Water,* vol. 4, no. 36, 2021. [CrossRef] [Google Scholar] [Publisher Link]

[10] Nimibofa Ayawei, Augustus Newton Ebelegi, and Donbebe Wankasi, "Modelling and Interpretation of Adsorption Isotherms," *Journal of Chemistry,* 2017. [CrossRef] [Google Scholar] [Publisher Link]

[11] Narandalai Byamba-ochir et al., "Highly Porous Activated Carbons Prepared from Carbon Rich Mongolian Anthracite by Direct NaOH Activation," *Applied Surface Science*, vol. 379, pp. 331-337, 2016. [CrossRef] [Google Scholar] [Publisher Link]

[12] Ranjihan Junejo et al., "Thermodynamic and Kinetic Studies for Adsorption of Reactive Blue (RB-19) Dye Using Calix [4] arene-Based Adsorbent," *Journal of Chemical & Engineering Data,* vol. 64, no. 8, pp. 3407-3415, 2019. [CrossRef] [Google Scholar] [Publisher Link]

[13] Ramsha Khan et al., "Environmental Contamination by Heavy Metals and Associated Human Health Risk Assessment : A Case Study of Surface Water in Gomti River Basin, India," *Environmental Science and Pollution Research,* vol. 28, pp. 56105-56116, 2021. [CrossRef] [Google Scholar] [Publisher Link]

[14] Ramesh Kumar, and Parimal Pal, "Lipase Immobilized Graphene Oxide Biocatalyst Assisted Enzymatic Transesterification of Pongamia Pinnata (Karanja) Oil and Downstream Enrichment of Biodiesel by Solar-driven Direct Contact Membrane Distillation Followed by Ultrafiltration," *Fuel Processing Technology*, vol. 211, 2021. [CrossRef] [Google Scholar] [Publisher Link]

[15] Samira Karimi, Mohammad Tavakkoli Yaraki, and Rama Rao Karri, "A Comprehensive Review of the Adsorption Mechanisms and Factors Influencing the Adsorption Process from the Perspective of Bioethanol Dehydration," *Renewable and Sustainable Energy Reviews*, vol. 107, pp. 535–553, 2019. [CrossRef] [Google Scholar] [Publisher Link]

[16] Samaila Muazu Batagarawa, and Lateefat Yusuf Dayo, "Millet Husk as Efficient Adsorbent for Removal of Lead, Cadmium, and Nickel Ions from Aqueous Solution," *Dutse Journal of Pure and Applied Sciences (DUJOPAS),* vol. 3, no. 1, pp. 337-348, 2017. [Google Scholar]

[17] Sirisha Nallakukkala et al., "Gas Hydrate-Based Heavy Metal Ion Removal from Industrial Wastewater: A Review," *Water,* vol. 14, no. 7, pp. 1-32, 2022. [CrossRef] [Google Scholar] [Publisher Link]

[18] V.S. Tatah et al., "Characterization and Adsorption Isotherm Studies of Cd (II) And Pb (II) Ions Bioremediation from Aqueous Solution Using Unmodified Sorghum Husk," *Journal of Applied Biotechnology & Bioengineering,* vol. 2, no. 3, pp. 113-120, 2017. [CrossRef] [Google Scholar] [Publisher Link]

[19] Zahia Harrache et al., "Thermodynamic and Kinetics Studies on Adsorption of Indigo Carmine from Aqueous Solution by Activated Carbon," *Microchemical Journal*, vol. 144, pp. 180-189, 2019. [CrossRef] [Google Scholar] [Publisher Link]